Ramond, J-B. et al. (2013). Selection of Clostridium spp. In biological sand filters neutralizing synthetic acid mine drainage.
FEMS Microbiology Ecology, 87: 678 – 690.
http://dx.doi.org/10.1111/1574-6941.12255

Selection of Clostridium spp. in biological sand filters neutralizing synthetic acid mine drainage

Jean-Baptiste Ramond, Pamela J. Welz, Marilize Le Roes-Hill, Marla I. Tuffin, Stephanie G. Burton & Don A. Cowan

Abstract

In this study, three biological sand filter (BSF) were contaminated with a synthetic iron- [1500 mg L^{-1} Fe(II), 500 mg L^{-1} Fe(III)] and sulphate-rich (6000 mg L^{-1} $SO^{2/4-}$) acid mine drainage (AMD) (pH = 2), for 24 days, to assess the remediation capacity and the evolution of autochthonous bacterial communities (monitored by T-RFLP and 16S rRNA gene clone libraries). To stimulate BSF bioremediation involving sulphate-reducing bacteria, a readily degradable carbon source (glucose, 8000 mg L^{-1}) was incorporated into the influent AMD. Complete neutralization and average removal efficiencies of 81.5 (±5.6)%, 95.8 (±1.2)% and 32.8 (±14.0)% for Fe(II), Fe(III) and sulphate were observed, respectively. Our results suggest that microbial iron reduction and sulphate reduction associated with iron precipitation were the main processes contributing to AMD neutralization. The effect of AMD on BSF sediment bacterial communities was highly reproducible. There was a decrease in diversity, and notably a single dominant operational taxonomic unit (OTU), closely related to *Clostridium beijerinckii,* which represented up to 65% of the total community at the end of the study period.

Introduction

Acid mine drainage (AMD) is one of the most environmentally threatening byproducts of the mining industry (Banks *et al.*, 1997; Akcil & Koldas, 2006; Kalin *et al.*, 2006). These sulphate-rich effluents are commonly characterized by an acidic pH and high concentrations of metals (e.g. iron, mercury, lead, copper) and/or metalloids (e.g. arsenic). The composition of AMD is, however, highly variable and depends on multiple factors: the geomorphology of the mining site (e.g. the presence of underground water network/s), temperature and climate, water and oxygen availability, the presence of oxidizing bacteria, the type of metals extracted and/or present *in situ*, and the presence/absence of metal sulphides and/or secondary minerals (e.g. aluminosilicates; Gazea *et al.*, 1996; Banks *et al.*, 1997; Akcil & Koldas, 2006; Hallberg, 2010). The treatment of AMD is therefore generally location specific, and a variety of biotic and abiotic remediation processes have been studied and developed (Gazea *et al.*, 1996; Johnson & Hallberg,

 don.cown@up.ac.za

2005a; Akcil & Koldas, 2006; Kalin *et al.*, 2006; Wilkin, 2008; Sheoran *et al.*, 2010; Macías *et al.*, 2012).

Biological treatment strategies for the remediation of AMD are classified as active (e.g. sulfidogenic bioreactors) or passive (e.g. (an)aerobic (constructed) wetlands, permeable reactive barriers, iron-oxidation bioreactors; Gazea *et al.*, 1996; Johnson & Hallberg, 2005a Akcil & Koldas, 2006; Kalin *et al.*, 2006). Active treatment systems involve the addition of neutralizing chemical agents to the AMD (e.g. limestone, NaOH, lime, $NaCO_3$) and necessitate the construction of treatment facilities on site (Gazea *et al.*, 1996). Passive treatment systems (PTS) are cost-effective and sustainable as they exploit naturally occurring (micro)biological processes/metabolisms and geochemical reactions, require less maintenance and have lower operational requirements than active systems (Gazea *et al.*, 1996; Johnson & Hallberg, 2005a; Cohen, 2006; Kalin *et al.*, 2006; Sheoran *et al.*, 2010). Therefore, PTS are ideal for the treatment of AMD in developing countries with mining-based economies such as South Africa.

In PTS such as biological sand filters (BSFs) or unplanted constructed wetlands, treatment of AMD is performed abiotically in the sediment matrix (*via* sorption, complexation, precipitation, dissolution of carbonates, abiotic reduction in iron oxides and (oxy) hydroxides) and biotically by microbially mediated reactions (sulphate/iron reduction, metal precipitation by microbially produced sulphides and biosorption; Cohen, 2006; Kalin *et al.*, 2006; McCauley *et al.*, 2009; Sheoran *et al.*, 2010; Burgos *et al.*, 2012). As abiotic removal processes ultimately have decreasing efficiencies due to the saturation of potential binding sites or the declining abundance of the 'precipitating/reducing-partner', it can be assumed that BSFs require an active community of sulphate-reducing bacteria (SRB) to achieve significant AMD treatment (Cohen, 2006; Sheoran *et al.*, 2010). These organisms actively participate in the neutralization and remediation of AMD by producing alkalinity (HCO^- ions) and sulphides, which immobilize metals and metalloid species in metal sulphide precipitates (Kim *et al.*, 1999; Kalin *et al.*, 2006; Wilkin, 2008; Sheoran *et al.*, 2010; Bai *et al.*, 2013).

In this study, the capacity of BSFs to remediate and neutralize synthetic AMD supplemented with an easily degradable carbon source (glucose) was evaluated. We hypothesized that such treatment would stimulate AMD bioremediation involving SRBs (Kim *et al.*, 1999; Sheoran *et al.*, 2010). We used molecular tools (terminal-restriction fragment length polymorphism [T-RFLP]/16S rRNA gene clone libraries) to study the responses of synthetic AMD-impacted microbial communities in four BSF ecological niches (inlet/outlet, surface/deep sediments). This approach offers an efficient and valid means of monitoring the diversity of micro-organisms capable of actively remediating AMD in BSFs and can be used to guide culturing strategies for the development of newly designed AMD treatment processes (Tyson *et al.*, 2005; Bai *et al.*, 2013).

Materials and methods

Experimental set-up and mode of operation of the BSFs

Four polyethylene tanks (length 173 cm/width 106 cm/ depth 30 cm) were set up as pilot-scale BSFs and operated in a mixed vertical and horizontal subsurface flow mode, that is, effluents were sprayed uniformly over the inlet zone allowing it to gravitate both longitudinally and vertically towards the outlet (Welz *et al.*, 2012). Each contained an equal quantity of river sand (*c.* 0.5 m^3) obtained from Malmesbury (South Africa). It was thoroughly hand-mixed with an inoculum of natural wetland sediment in a 1 (wetland sediment) to 4 (river sand) ratio as previously described (Ramond *et al.*, 2012). The inoculum was harvested in a zone where no plant growth was observed and corresponded to the first 10 cm. The final BSF sediment composition consisted of 1% clay, 7% silt, 4% fine sand, 12% medium sand and 76% coarse sand. The hydraulic retention times of the BSFs were estimated to be 22 days, thus were functioning as slow sand filters (Haig *et al.*, 2011). Prior to amendment with synthetic AMD (this study), the four BSFs were fed biweekly with basal nutrients consisting of 0.3 g glucose and 0.3 g yeast extract in 12.5 L tap water for a period of 100 days as previously (Ramond *et al.*, 2012). It has been shown that this procedure results in the establishment of similar microbial community patterns in surface and subsurface sediments of replicate BSFs, thereby ensuring the relevance of subsequent experimental comparisons (Ramond *et al.*, 2012, 2013). This nutrient-feeding regime was designed to provide a concentration-based C : N : P ratio of 32:7:1, with a low carbon supply (influent COD = 24 mg L^{-1}) and non-limited nitrogen (N) and phosphorous (P) sources, with 5.5 and 0.76 mg L^{-1} of total N and total P in the influent, respectively.

Thereafter, all four BSFs were fed on a weekly basis with the same 12.5 L basal nutrient solution. BSF A was designated as the control and BSFs B, C and D as experimental systems and amended with synthetic AMD (pH = 2) containing 500 mg L^{-1} magnesium ions (Mg^{2+}), 1500 mg L^{-1} Fe(II), 500 mg L^{-1} Fe(III) and 6000 mg L^{-1} sulphate ions ($SO^{2/4-}$; Table 1; Potgieter-Vermaak *et al.*, 2006). To provide sufficient carbon electron donors for the SRB, a high concentration of glucose (8000 mg L^{-1}) was also added to the synthetic AMD. The amount of glucose was estimated using the stoichiometric requirements for total sulphate reduction according to eqn 1. The COD/sulphate ratio used was equal to 1.4, which is higher than previously suggested (0.67–1; Reifler *et al.*, 2008; Mulopo *et al.*, 2011).

$$C_6H_{12}O_{6(s)} + 3SO^-_{4(aq)} \rightarrow 3H_2S_{(g)} + 6HCO^-_{3(aq)} \qquad (1)$$

Both for the 3-month establishment period and the AMD exposure experiment, the effluent distribution rate was of 0.68 L min^{-1} (Ramond *et al.*, 2012).

Sediment sampling and characterization

A 30-mm-diameter PVC sediment corer was used to recover samples without major disturbance of the sediment stratification. One hour after the end of the effluent distribution, triplicate sample cores were taken from the inlet and the outlet of each BSF, at the start (Day 0, D0) and the end of the experiment (Day 24, D24). The saturated surface (0–3 cm) and deep (15–20 cm) sediment subsamples were pooled according to their BSF origin (inlet/outlet). After homogenization, the composite subsamples were frozen at -80 °C for subsequent molecular analysis (1 g wet weight sediment) or chemical analyses.

Table 1. Average influent and effluent wastewater parameter and removal rates of the synthetic AMD-amended BSFs BCD after 24 days of operation

Parameter	Influent	Effluent	Removal (%)
pH	2	6.2 ± 0.1	N.A.
Redox (mV)	399.5 ± 30.3	118.0 ± 13.0	N.A.
Sulphate (mg L^{-1})	6000.0	4033.3 ± 838.7	32.8 ± 14.0
Iron(II) (mg L^{-1})	1500.0	278.0 ± 84.0	81.5 ± 5.6
Iron(III) (mg L^{-1})	500.0	21.0 ± 6.1	95.8 ± 1.2
COD (mg L^{-1})	8520.0	3515.0 ± 853.8	58.7 ± 10.0

N.A., not applicable.

$$\text{Removal efficiency}\,(\%) = 100 \times \left(100 - \frac{\text{BSF BCD effluent concentration} - \text{BSF A effluent concentration}}{\text{BCF BCD influent concentration}}\right).$$

Table 2. Evolution of the BSFs' sediment characteristics after 24 days of operation

	Surface sediments [inlet/outlet]				Deep sediments [inlet/outlet]			
	BSF A	BSF B	BSF C	BSF D	BSF A	BSF B	BSF C	BSF D
pH								
Day 0	7.8/7.8	7.8/7.8	8.0/8.0	7.6/7.6	7.5/7.5	7.8/7.8	7.8/7.8	7.4/7.4
Day 24	7.7/7.7	7.9/7.7	8.0/8.0	7.6/7.2	8.0/8.2	8.1/7.8	8.2/8.1	7.1/7.6
Total S (mg kg^{-1})								
Day 0	5.3/5.3	5.0/5.0	5.1/5.1	20.7/20.7	4.9/4.9	8.0/8.0	10.1/10.1	7.0/7.0
Day 24	24.9/8.9	118.6/170.7	72.5/88.8	105.5/104.4	8.7/10.4	17.67/25.2	17.61/19.1	31.67/12.2
Total Fe (mg kg^{-1})								
Day 0	872.2/872.2	470.2/470.2	243.3/243.3	459.6/459.6	633.7/633.7	1217.7/1222.7	837.7/833.7	575.3/575.3
Day 24	490.6/735.4	1107.9/1045.6	804.8/668.5	946.0/777.2	512.0/498.3	558.0/999.5	554.3/1043.6	1645.4/1388.2
Total C (%)								
Day 0	0.07/0.07	0.10/0.10	0.10/0.10	0.18/0.18	0.10/0.10	0.21/0.21	0.11/0.11	0.23/0.23
Day 24	0.16/0.25	0.11/0.10	0.21/0.19	0.23/0.11	0.10/0.12	0.17/0.23	0.25/0.16	0.20/0.21
Total N (%)								
Day 0	0.07/0.07	0.07/0.07	0.07/0.07	0.07/0.07	0.06/0.06	0.06/0.06	0.06/0.06	0.06/0.06
Day 24	0.10/0.14	0.12/0.09	0.08/0.05	0.07/0.05	0.17/0.10	0.10/0.09	0.06/0.10	0.08/0.07

Micronutrient element levels were determined using a Varian® MPX ICP-OES spectrophotometer (Agilent Technologies, Santa Clara) and consisted of 1.9 g kg^{-1} C, 6 mg kg^{-1} P, 16.1 mg kg^{-1} Na, 19.5 mg kg^{-1} K, 328 mg kg^{-1} Ca, 50.4 mg kg^{-1} Mg, 0.61 mg kg^{-1} Cu, 1.0 mg kg^{-1} Zn, 1.9 mg kg^{-1} Mn, 0.10 mg kg^{-1} B, 63.03 mg kg^{-1} Fe and 7.42 mg kg^{-1} S.

XRF (X-ray fluorescence) analysis was performed to determine the elemental composition of the BSF sediments before and after AMD exposure by initially crushing and milling the sediments into fine powder with clean jaw crushers and a tungsten zib mill, respectively. XRF spectrometry was performed on a PANalytical Axios Wavelength Dispersive spectrometer (PANalytical, Netherlands) at the Central Analytical Facilities of Stellenbosch University (South Africa). Control standards

were NIM-G (granite from the Council for Mineral Technology, South Africa) and BHVO-1 (basalt from the United States Geological Survey).

XRD (X-ray diffraction) analysis was used to assess the crystalline structure of the BSF sediments. A small amount (1–2 g) of sediment was crushed into a fine powder, placed in a sample holder and subjected to XRD analysis. The instrument used was a Philips PW 1390 XRD (Department of Geological Sciences, University of Cape Town, South Africa), which uses a copper K-a X-Ray tube with x-ray wavelength of 1.542 A, accelerating voltage = 40 kV and current = 25 mA. Bragg 2Θ angles between 2 and 70° were used for analysis. A continuous scan step size of 0.02° was applied with a scan step time of 0.4 s. The resultant XRD spectra '2Θ vs intensity' was entered in the software X'Pert and the d-spacing of the most intense peaks calculated by solving for the Bragg equation.

The pH, total carbon (C), total nitrogen (N), total iron (Fe) and total sulphur (S) contents of sediment samples were analysed by Bemlab (Pty) Ltd (Strand, Western Cape, South Africa; Table 2). The neutralizing potential of the sediment was determined as $CaCO_3$ equivalents (eq.) and were measured by titration with HCl according to standard methods (Bundy & Bremner, 1972).

Metagenomic DNA extraction

Total DNA from the BSF sediment core samples was extracted from 0.3 g (wet weight) using the Powersoil® DNA isolation kit according to the manufacturer's instructions (MOBIO laboratories, San Diego). Metagenomic DNA concentrations were estimated with a NanoDrop spectrophotometer (NanoDrop Technologies, Montchanin, DE).

PCR amplification, purification and restriction digestion

All polymerase chain reactions (PCRs) were carried out in a Bio-Rad Thermocycler (T100™ Thermal Cycler). Bacterial 16S rRNA-encoding genes were amplified using the universal bacterial primers E9F (5′-GAGTTT GATCCTGGCTCAG-3′) and U1510R (5′-GGTTACCTTGTTACGACTT-3′; Reysenbach & Pace, 1995; Marchesi *et al.*, 1998). PCR was carried out in 50 lL reaction volumes. Each reaction contained 19 PCR buffer, 0.2 U Dream*Taq*™ polymerase (Fermentas), 200 lM of each dNTP, 0.5 lM of each primer, 0.1% bovine serum albumin (BSA) and between 10 and 20 ng of metagenomic DNA. PCR amplification was carried out as follows: 4 min at 94 °C for denaturation; 30 cycles of 30 s at 94 °C, 30 s annealing at 52 °C and 105 s at 72 °C; and a final elongation step of 10 min at 72 °C.

To perform T-RFLP analyses, the E9F primer was 5′- end FAM-labelled and the PCR products were purified using the GFX™ PCR DNA and gel band purification kit as directed by the supplier (GE Healthcare, UK). Purified PCR products (200 ng) were digested with the restriction enzyme HaeIII at 37 °C overnight.

T-RFLP analysis

The bacterial community structure was assessed by T-RFLP fingerprinting using the 16S rRNA gene as a marker. The precise length of T-RFs was determined by capillary electrophoresis using the Applied Biosystems DNA Sequencer 3130 (Applied Biosystems, Foster City, CA) and according to the molecular weight standard Rox1.1 (with an acceptable error of ±1 bp). T-RFLP patterns and quality were analysed using the freeware PeakS-canner^{TM} (version 1.0; Applied Biosystems, https:// products.appliedbiosystems.com). Individual T-RFs were considered as operational taxonomic units (OTUs), with recognition that each OTU may comprise more than one distinct bacterial ribotype (Nocker *et al.*, 2007). Peak height was used to identify each unique T-RF and characterize their relative abundance in the total T-RFLP profiles, which was used as a proxy of OTU abundances in the BSF bacterial populations (Osborn *et al.*, 2000). *In silico* identification of AMD-selected T-RFs was performed using clone libraries. A ±2 bp size margin, lower than that previously recommended (±3 bp; Sercu *et al.*, 2011), was implemented to take into account potential differences between real and predicted T-RFs.

Bacterial 16S rRNA gene clone libraries construction and phylogenetic analysis

Two clone libraries were constructed after pooling equal amounts of the inlet and outlet amplicons from the surface or deep samples of the AMD-contaminated BSFs. The pooled PCR products were cloned into *Escherichia coli* DH5a using a pGEM-T cloning kit (Promega, Madison, WI). One hundred and ninety two transformants per clone library were selected by blue–white screening. The presence of correctly sized inserts was confirmed by colony PCR (using M13F/R primers). Amplified rDNA restriction analysis (ARDRA; using HaeIII and AluI) was used to dereplicate clones. Restriction patterns were visualized on 2.5% agarose gels, and PCR products with unique ARDRA patterns were sequenced using the vector primer M13F with an ABI 3130 DNA Sequencer (Applied Biosystems). Chimeric sequences were filtered using Bellerophon (Huber *et al.*, 2004). Phylogenetic OTUs (97% similarity cut-off) were determined using CD-Hit (Huang *et al.*, 2010). The phylogenetic tree was constructed with MEGA5 (Tamura *et al.*, 2011) using the neighbour-joining method (Saitou & Nei, 1987). The robustness of the tree topology was evaluated by boot-strap analysis based on 1000 replicates (Felsenstein, 1985). The genetic distances were calculated using Kimura's 2-parameter model (Kimura, 1980). Sequences obtained in this study were deposited in the NCBI GenBank database under accession numbers KC701527–KC701593 and their taxonomic classification obtained using the online aligner SINA with the default parameters (Pruesse *et al.*, 2012; Supporting Information, Tables S1 and S2).

Statistical analyses

Multivariate analyses of T-RFLP or environmental data were carried out using the software PRIMER 6 (Primer-E Ltd, UK). Valid T-RF peaks (between 35 and 1000 bp) from triplicate T-RFLP profiles were identified, compiled and aligned to

produce large data matrices using the online software T-REX (http://trex.biohpc.org/; Culman *et al.*, 2009). T-RFs with intensities lower than 0.5%, which may have originated from background interference, were excluded from the matrices. The community structures obtained were analysed by ordination using non-metric multidimensional scaling (nMDS) of Bray–Curtis similarity matrices of untransformed data. An analysis of similarity (ANOSIM), performed on the resemblance matrix, was used to test for differences in bacterial community structure between predefined groups (Clarke, 1993).

The environmental data presented in Table 2 were normalized prior to analysis by principal component analysis (PCA). A resemblance matrix based on Euclidean distance was created using the normalized variables prior to ANOSIM.

Results

Effectiveness of synthetic AMD remediation by BSFs

Near-complete neutralization of the synthetic AMD was achieved, with an average BSF effluent pH of 6.2 (±0.1) (Table 1), and with neutral to slightly alkaline sediment pH, ranging from 7.2 (surface outlet BSF B) to 8.2 (surface outlet BSF B and deep inlet BSF C; Table 2). Removal efficiencies of 81.5 (±5.6)%, 95.8 (±1.2)% and 32.8 (±14.0)% for Fe(II), Fe(III) and sulphate, respectively, were observed concomitantly with a decrease in effluent redox potential (from 399.5 mV (±30.3) to 118.0 mV (±13.0); Table 1).

BSF sediment characterization

XRD analysis demonstrated that the spectrum of the BSF sediments matched with that of quartz (a mineral form of Si; Supporting Information, Fig. S1a) and not with reference spectra of carbonates (Calcite [$CaCO_3$] and Dolomite [$CaMg(CO_3)_2$]) (Fig. S1b) or aluminosilicates (chabazite, offretite, kyanite and sillimanite; Fig. S1c). XRF analyses showed that the BSF sediments were constituted predominantly of silica (SiO_2; 96.51% and 95.72% at Day 0 and Day 24, respectively), with small amounts of Al_2O_3 (0.82%/0.90%), Fe_2O_3 (0.33%/0.42%), TiO_2 (0.07%/0.12%), CaO (0.02%/0.30%), K_2O (0.02%/0.03%) and P_2O_5 (0.01%/0.01%), and did not change during the experiment. In addition, neutralizing capacity, determined as $CaCO_3$ eq, was also initially low (4.1%) and only decreased to 2.8% $CaCO_3$ eq after 24 days. Such composition was indicative of poor neutralizing potential.

The PCA ordination of the environmental variables presented in Table 2 is presented in Fig. 1. For the surface sediment variables, 61.4% of the data variability is shown, with PC1 explaining 39.2% and PC2 22.2% (Fig. 1a). For the deep sediments, 68.3% of the data variability is explained, with PC1 accounting for 40.6% and PC2 27.8% (Fig. 1b). In both sedimentary compartments, ANOSIM showed that the Day 24 sediments of the AMD-impacted BSFs were significantly different to those of the control BSF A Day 24 samples and the Day 0 samples of the four BSFs [R = 0.578 (P = 0.001) or

0.359 (P = 0.002) for the surface or the deep sediments, respectively], demonstrating that AMD altered the BSF sediment chemistry. Notably, total S and Fe increased significantly in the surface sediments of BSFs B, C and D during the course of the experiment (Table 2). However, no spatial effect of AMD was demonstrated when comparing inlet and outlet sediment chemistries of the AMD-contaminated BSFs (ANOSIM, P > 0.4).

Bacterial community structure evolution

The nonmetric multidimensional scaling (nMDS) plots displayed in Fig. 2 show clustering of the bacterial com- munities derived from the surface (Fig. 2a) and deep (Fig. 2b) sediments at Day 0, indicating that the equili- bration procedure yielded similar communities in each BSF prior to initiating the experiment (Ramond *et al.*, 2012). After 24 days of exposure to synthetic AMD, the bacterial communities in the sediments were drastically modified (Fig. 2a and b), as indicated by the elevated (1 and 0.922 for the surface and deep sediments, respec- tively) and highly significant (P = 0.002) ANOSIM global R value (Fig. 2a and b). Apart from the communities at the surface inlet of BSF B (Fig. S2a), a less diverse commu- nity evolved within the 24-day experimental period in each microenvironment of the test BSFs (Figs S2b and S3). In the synthetic AMD-exposed BSF sediments, eight OTUs from surface samples, with sizes of 212, 219, 220, 226, 297, 406, 609, 893 bases (Fig. 3), and three OTUs from deep samples, with sizes of 297, 406 and 893 bases (Fig. 4), responded to exposure to AMD; that is, detected in the communities of the test BSFs B, C and D and not in the control BSF A. In particular, the 297 base OTU was consistently selected, becoming the dominant mem- ber (27.2% to 64.6%) of the bacterial community in each niche.

16S rRNA gene clone libraries were constructed to identify members of the bacterial communities that were selected upon exposure to the synthetic AMD. A total of 128 clones were sequenced, 62 from DNA extracted from the surface sediments and 66 from DNA extracted from the deep sediments. The phylogenetic tree presented in Fig. 5 shows that a high diversity of bacterial sequences was retrieved from the synthetic AMD-impacted BSF sediments. Black-starred sequences in Fig. 5 are related to clones or bacteria isolated from sites similar to AMD-impacted environments (i.e. acidic, iron-rich, metal-contaminated environments), while grey-starred sequences are related to bacterial species (or genera) with relevant ecosystem functions. Clones related to primary producers, that is, photolithotrophic sulphur oxydizers (*Chlorobium* sp., clone D24) and photosynthetic cyano- bacteria (clones S44 and S138), were observed. Similarly, the presence of clones related to bacteria involved in the N cycle was noted, with N-fixers (*Azotobacter* spp., clones D147 and S114) and potential denitrifiers (*Steroidobacter denitrificans*, clone D114) detected.

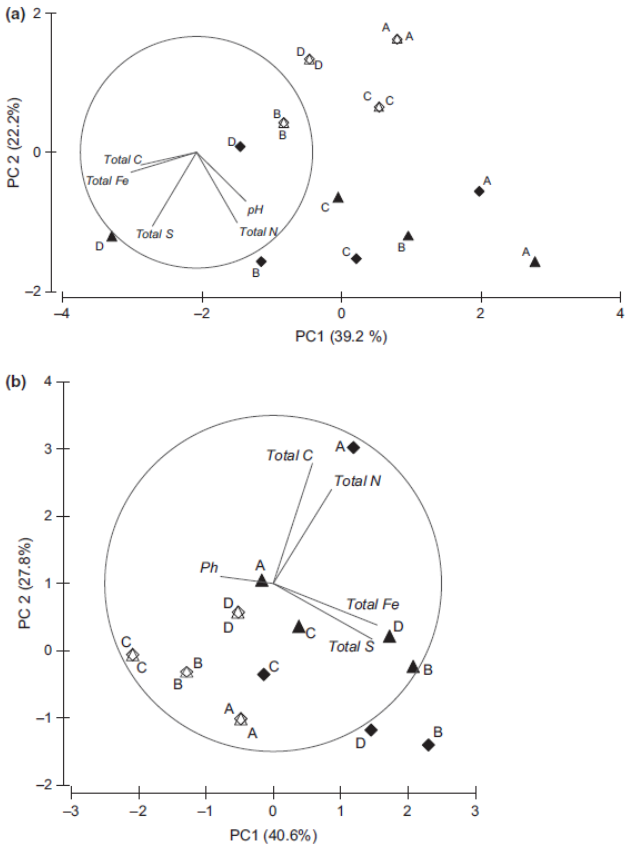

Fig. 1. Principal component analysis (PCA) plot of the normalized BSF environmental variables presented in Table 2. (a) BSF surface sediment. (b) BSF deep sediment. Letters A, B, C and D refer to the respective BSFs.Δ: Inlet Day 0; ▲: Inlet Day 24; ◇: Outlet Day 0; ♦: Outlet Day 24.

In addition, a great variety of heterotrophs were detected probably in relation with the important glucose content added to the synthetic AMD. Sequences close to those of bacteria involved in the S and Fe cycles were also observed. These include (1) *Chlorobium* spp. that can utilize sulphides ($S^{2/4-}$, HS^-) as electron donors (clone D24), (2) SRB that utilize sulphate as electron acceptor and generate volatile H_2S (clone D80), (3) the sulphur oxidizer and Fe(III) reducer *Geobacter* sp. (clone D73) and (4) the sulphite (SO^{2-}) reduc- ers *Clostridium* spp. such as *Clostridium vincentii* (clone S159) and *Clostridium beijerinkii* (clones D42, D93, S106 and S161; Fig. 5; Tables S1 and S2).

Clones with sequences potentially related to the eight AMD-selected OTUs detected by T-RFLP (black-starred in Figs 3 and 4) were also observed (underlined in Fig. 5, and determined with a ±2 bp margin lower than that recommended previously; Sercu *et al.*, 2011). They were found to be related to b-proteobacteria (OTUs 219 and 220), the candidate division TM7 (OTU 212), *Chlorobium* spp. (OTU 406), Bacteroidetes (OTUs 609 and 893), Firmicutes (OTUs 212, 219, 220 and 297) and Actinobacteria (OTU 226). As OTUs 212, 219 and 220 were related to distinct bacterial phyla, it confirmed that in T-RFLP studies, an OTU may correspond to more than one distinct bacterial ribotype (Nocker *et al.*, 2007) and that extreme care must be taken when phylogenetically assigning T-RFs. Sequences assigned to the dominant OTU 297 (Figs 3 and 4) were, however, only closely related to *Clostridium beijerinckii* (Fig. 5).

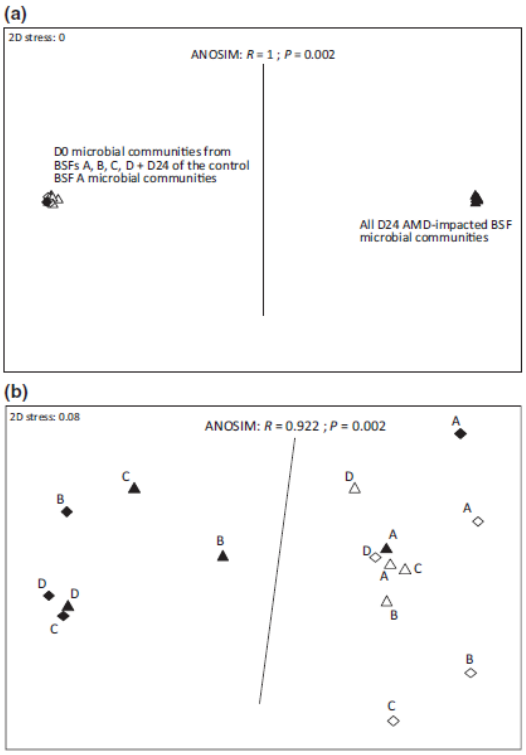

Fig. 2. 2D-Nonmetric multidimensional scaling plot of Bray–Curtis similarity of bacterial community structures based on 16S rRNA gene T-RFLP profiles. (a) BSF surface sediment microbial communities. (b) BSF deep sediment microbial communities. Letters A, B, C and D refer to the respective BSFs. Δ: Inlet Day 0; ▲: Inlet Day 24; ◇: Outlet Day 0; ♦: Outlet Day 24. The black line virtually separates significantly different communities as revealed by ANOSIM analysis. D24: Day 24.

The taxonomic classification of the 16S rRNA gene sequences of the individual clones, obtained using the online aligner SINA (Pruesse *et al.*, 2012), is presented in Tables S1 and S2 for the surface and deep sediments, respectively. The per cent identity of these sequences was generally low, that is, < 97% (22/32 and 18/29 in Tables S1 and S2, respectively), indicating that they potentially belong to novel species and possibly to new phyla (< 85%; 3/32 and 3/29 in Tables S1 and S2; Hugenholtz *et al.*, 1998). However, given the general shortness of the sequences obtained (ranging from 362 to 633 bp; Tables S1 and S2), to ascertain the discovery of novel bacterial phyla (and even genera), the full length of the cloned 16S rRNA gene should be sequenced. These results strongly suggest that AMD contamination induced selection of specific bacterial communities with highly novel compositions.

Discussion

AMD neutralization in BSFs

In BSFs, the sediment matrix and the microbial communities are responsible for the remediation performance (Welz *et al.*, 2012). As sediments with similar elemental and crystal composition to those used in this study have low neutralizing capacity, the major AMD neutralization process(es) taking place in BSFs B, C and D were (1) microbial in origin, involving iron and/or sulphate reduction (Wilkin, 2008; Sheoran

et al., 2010), and/or (2) linked to precipitation (Fe and S) and adsorption (Fe) reactions. The latter is clear from the fact that the total Fe and S concentrations in the AMD-impacted BSF surface sediments increased (Table 2). Indeed, (1) precipitation of ferric ions (Fe^{3+}) occurs under slightly alkaline conditions (as observed for the BSF sediments, Table 2) in the form of oxyhydroxides (Grundl & Delwiche, 1993; Kalin *et al.*, 2006), and (2) ferrous ions (Fe^{2+}) can also precipitate in the form of FeS and $FeCO_3$ when reacting with HS^- and HCO^-, two end products of microbial sulphate reduction (Sheoran *et al.*, 2010).

The important Fe(III) removal efficiency (95.8 ± 1.2%) also suggested microbial iron reduction activity as Fe^{3+} is widely used as an electron acceptor by micro-organisms or as a terminal electron acceptor in dissimilatory iron reduction (Schroder *et al.*, 2003). The lower Fe(II) removal efficiency (81.5 ± 5.6%) observed could therefore result from the fact that it is released by both these processes. The decrease in sulphate concentration and redox potential was indicative of bacterial sulphate reduction (Table 1; Johnson & Hallberg, 2005b), which is supported by the fact that the sediment pH values were compatible with sulphate-reducing conditions (pH = 5–8; Sheoran *et al.*, 2010).

This important disparity in removal efficiencies (i.e. elevated iron removal and low sulphate removal) indicated that iron reduction was the principal microbial neutralizing process. These results are consistent with previous reports suggesting that in AMD-treating bioreactors, sulphate reduction only occurred after Fe^{3+} was actively reduced to Fe^{2+} (Kalin *et al.*, 2006). While other microbial processes, such as denitrification, methanogenesis and/or ammonification, may also have been implicated (Johnson & Hallberg, 2002; Kalin *et al.*, 2006), we did not monitor these chemistries. Notably, as nonlimited N was supplied to the BSFs, denitrification cannot be excluded as this microbially mediated neutralizing process consumes protons and releases volatile N_2 (Kalin *et al.*, 2006), and denitrifiers were identified (*Steroidobacter denitrificans*, clone D114; Fig. 5).

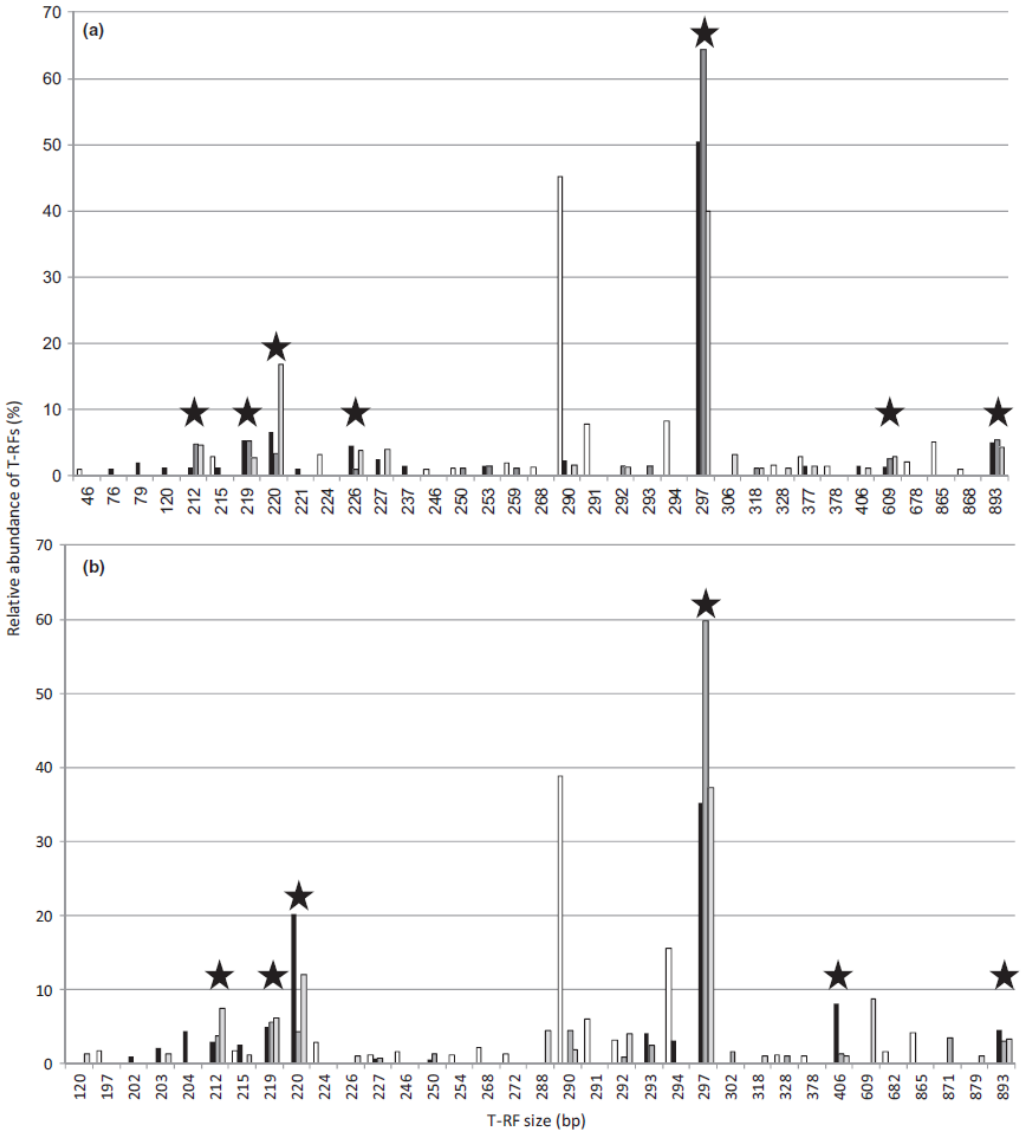

Fig. 3. Relative abundance and contribution to total fluorescence of individual peak in the BSF surface sediment T-RFLP profiles after 24 days of AMD exposure. (a) Surface inlet. (b) surface outlet. □: control BSF A; ■: BSF B; ■: BSF C; ■: BSF D. ★: AMD-selected T-RFs in the three impacted BSFs (B, C, D). Only T-RFs with relative abundances higher than 1% are represented.

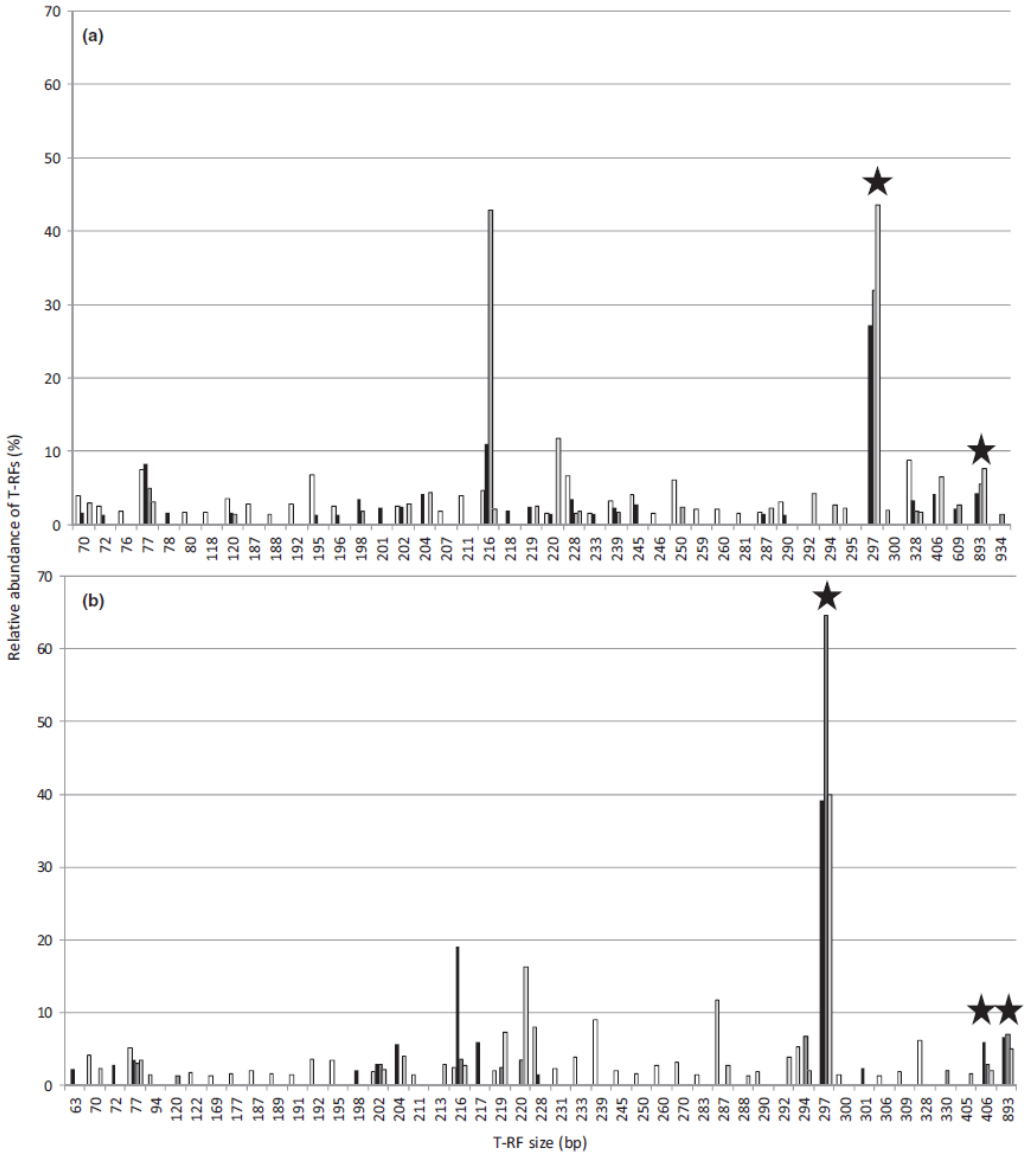

Fig. 4. Relative abundance and contribution to total fluorescence of individual peak in the BSF deep sediment T-RFLP profiles after 24 days of AMD exposure. (a) Deep inlet. (b) deep outlet. □: control BSF A; ■: BSF B; ▩: BSF C; ▨: BSF D. ★: AMD-selected T-RFs in the three impacted BSFs (B, C, D). Only T-RFs with relative abundances higher than 1% are represented.

Adaptation of BSF bacterial communities to AMD exposure

This study provided evidence that microbially mediated mechanisms were involved in the neutralization of the synthetic AMD as well as iron and sulphate removal in the BSFs. The identification of bacterial phyla/communities that may have been responsible for iron/and or sulphate reduction was therefore assessed at the end of the AMD supplementation process. In this study, we focused on bacterial communities as they constitute the main contributors to microbially mediated AMD treatment processes (Kim *et al.*, 1999; Sheoran *et al.*, 2010; Bai *et al.*, 2013), even though members from the complete microbial tree of life (i.e. eucarya, bacteria and archaea) have been identified and characterized in acidophilic communities (Baker & Banfield, 2003).

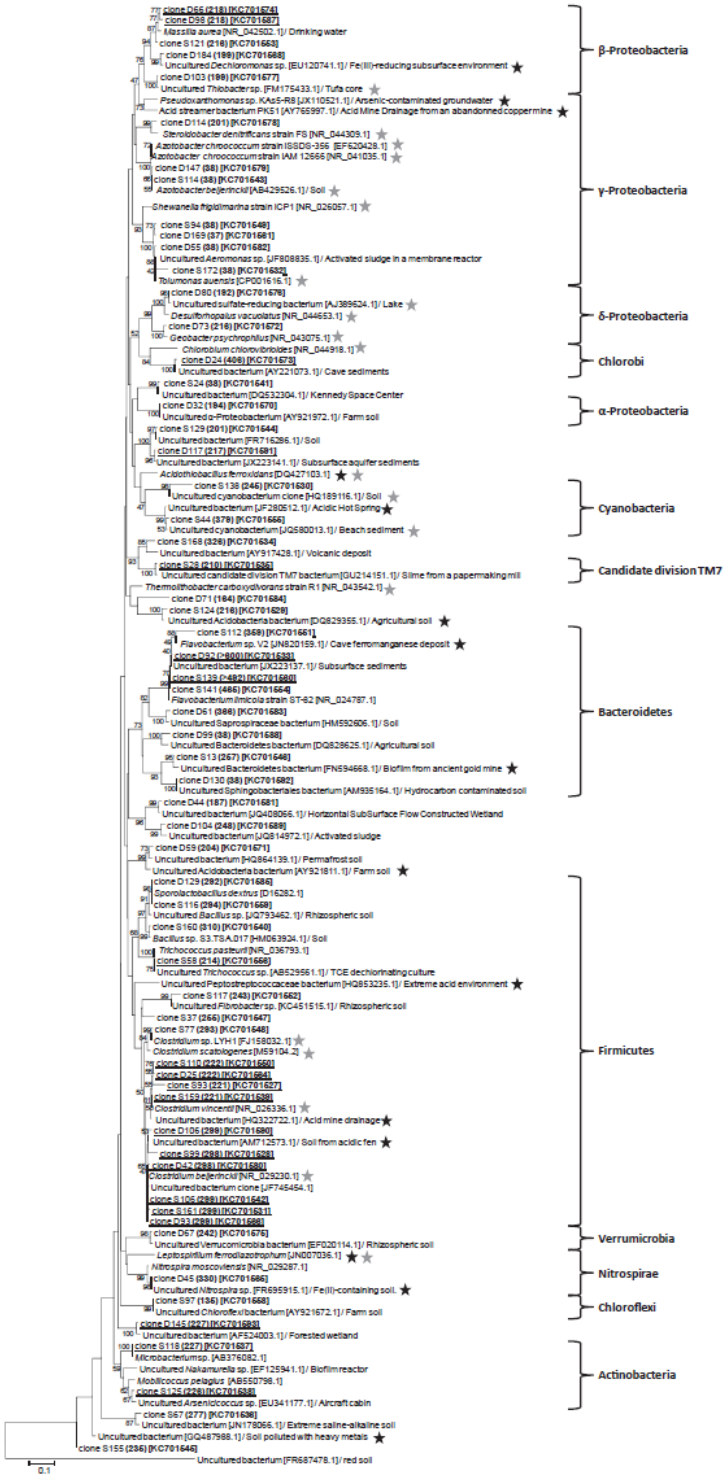

Fig. 5. Neighbour-joining tree of representative 16S rRNA gene sequences from clone libraries of AMD-contaminated BFS sediments. S: surface/ D: deep. The respective *in silico* T-RF sizes with the restriction enzyme HaeIII (used to perform T-RFLP) are indicated by bold font. The underlined clones possess matching HaeIII T-RFs sizes of interest (black-starred in Figs 3 and 4). ★: matching sequences or micro-organisms retrieved from relevant environments. ☆: micro-organisms with relevant metabolisms. Only bootstrap values ≥ 40% are shown. Bar: 0.1 substitutions per nucleotide position.

AMD contamination led to severe community structure alteration. This was not unexpected, as microbial assemblages in acidic environments exhibit low species richness compared with neutral environments (Baker & Banfield, 2003). Moreover,

acidic conditions and elevated iron and sulphate concentrations are known to select for highly specialized microbial communities (Baker & Banfield, 2003; Allen & Banfield, 2005). Such adaptive traits of microbial communities impacted by highly toxic effluents have been previously reported in metal-contaminated sediments (e.g. mercury; Ramond *et al.*, 2009) and AMD-impacted biofilms (Edwards *et al.*, 2000), underlining the fact that extreme abiotic environmental factors vigorously control bacterial community structures and composition (Allen & Banfield, 2005).

The newly selected members of the BSF communities were adapted to the selective pressure imposed by the acidic conditions and high iron and sulphate concentrations of the synthetic AMD, that is, by having physiological traits that allowed them to both withstand these newly imposed extreme conditions while maintaining the essential ecosystem functions (Allison & Martiny, 2008). This is very apparent from our detection of sequences related to primary producers and N-fixers and also sequences from bacteria shown to actively participate in S and Fe cycling at the end of the AMD treatment period. The latter particularly included members of the polyphyletic Clostridia class, which have been shown to actively participate in S and Fe cycling (Harrison *et al.*, 1984; Dobbin *et al.*, 1999), notably, *C. beijerinkii* (sulphites and Fe(III) reducer), *C. vincentii* (sulphite reducer), and Gram- positive spore-forming cluster III SRB, which are closely related to Clostridiales and able to perform dissimilatory sulphate reduction (Castro *et al.*, 2000). It is noteworthy that the dominant AMD-selected OTU 297 was found to be closely related to *C. beijerinkii* (sulphite and Fe(III) reduction; Dobbin *et al.*, 1999). This finding may represent an important breakthrough for the design of microbially mediated AMD treatment systems, and its isolation recommended. Furthermore, the fact that *c.* 10% of the sequences retrieved from the clone libraries presented < 85% identity with known sequences is remarkable and indicates that AMD-contaminated environments and AMD biological treatment systems represent ideal environments to discover highly novel micro-organisms with AMD treatment potential.

Conclusions

This study demonstrated that the principal effect of synthetic AMD amendment on the BSF sediment bacterial communities was a rapid and drastic shift in community composition. This effect was reproducible in all three experimental systems. Similarly, in all systems, there was a decrease in bacterial diversity and the consistent selection of at least one dominant OTU. Many of the selected bacterial phylotypes potentially exhibited a range of metabolic processes that had the capacity, at a community level, to neutralize and decontaminate an acidic, iron- and sulphate-rich AMD and also to perform many of the functions that contribute to the stability of the BSFs' ecosystems (notably primary production and N-fixation). The selection of *Clostridia*-like sequences as dominant members of the bacterial communities in the four BSF niches studied is also remarkable. It strongly suggests that members of this polyphyletic group actively participate in BSF AMD

neutralization and should be more considered when designing AMD biological treatment systems.

Given that a 24-day experimental period is too short to provide evidence of sustainability, the presence of these phylotypes is suggestive of microbial processes, which may support system stability and long-term remediation performance. However, the testing of BSFs as an alternative biological AMD treatment system should be continued by (1) extending the operational time, (2) testing for alternative and cheaper C source/electron donor than glucose (e.g. acetate or ideally another readily available wastewater; Kargu & Uygur, 2003; Obaja *et al.*, 2005) and *in fine* by (3) using real AMD or synthetic AMD artificially concentrated in heavy metals. Indeed, the inherent metallic composition of AMD may severely affect the composition of the BSF indigenous communities (and by extension their resistance and resilience to AMD; Allison & Martiny, 2008), thereby resulting in inferior AMD neutralization to that achieved in this study. Nevertheless, the novelty of the bacterial 16S rRNA gene sequence obtained in this study emphasizes the fact that biological AMD treatment processes should be more carefully monitored and/or be used as incubators to select for novel micro-organisms with potential biotechnological applications, particularly in AMD remediation. Finally, it must be noted that iron reduction rather than the originally hypothesized sulphate reduction was the principal microbial neutralizing process in these BSF systems.

Acknowledgements
This study was funded by the Water Research Commission of South Africa (WRC project K5/2104). J-BR held a Free-standing Postdoctoral Fellowships from the National Research Foundation (NRF) of South Africa. Dr Bronwyn Kirby (Next Generation Sequencing Unit, University of the Western Cape, Cape Town, South Africa) is acknowledged for assisting in the analysis of the clone libraries.

Statement
The BSF bacterial community composition was drastically altered by AMD, with the predominant selection of sequences related to *Clostridium* spp.

References

Akcil A & Koldas S (2006) Acid mine drainage (AMD): causes, treatment and case study. *J Clean Prod* 14: 1139–1145.

Allen EE & Banfield JF (2005) Community genomics in microbial ecology and evolution. *Nat Rev Microbiol* 3: 489–498.

Allison SD & Martiny JBH (2008) Resistance, resilience, and redundancy in microbial communities. *P Natl Acad Sci USA* 105: 11512–11519.

Bai H, Kang Y, Quan H, Han Y, Sun J & Feng Y (2013) Treatment of acid mine drainage by sulfate reducing bacteria with iron bench scale runs. *Bioresour Technol* 128: 818–822.

Baker BJ & Banfield JF (2003) Microbial communities in acid mine drainage. *FEMS Microbiol Ecol* 44: 139–152.

Banks D, Younger PL, Arenese R-T, Iversen ER & Banks SB (1997) Mine water chemistry: the good, the bad and the ugly. *Environ Geol* 32: 157–174.

Bundy LG & Bremner JM (1972) A simple titrimetric method for determination of inorganic carbon in soils. *Soil Sci Soc Am J* 36: 273–275.

Burgos WD, Borch T, Troyer LD, Luan F, Larson LN, Brown JF, Lambson J & Shimizu M (2012) Schwertmannite and Fe oxides formed by biological low-pH Fe(II) oxidation versus abiotic neutralization: impact on trace metal sequestration. *Geochim Cosmochim Acta* 76: 29–44.

Castro HF, Williams NH & Ogram A (2000) Phylogeny of sulfate-reducing bacteria. *FEMS Microbiol Ecol* 31: 1–9.

Clarke K (1993) Non-parametric multivariate analysis of changes in community structure. *Aust J Ecol* 18: 117–143.

Cohen RRH (2006) Use of microbes for cost reduction of metal removal from metals and mining industry waste streams. *J Clean Prod* 14: 1146–1157.

Culman SW, Bukowski R, Gauch HG, Cadillo-Quiroz H & Buckley DH (2009) T-REX: software for the processing and analysis of T-RFLP data. *BMC Bioinformatics* 10: 171.

Dobbin PS, Carter JP, San Juan CG-S, von Hobe M, Powell AK & Richardson DJ (1999) Dissimilatory Fe(III) reduction by *Clostridium beijerinckii* isolated from freshwater sediment using Fe(III) maltol enrichment. *FEMS Microbiol Lett* 176: 131–138.

Edwards KJ, Bond PL, Gihring TM & Banfield JF (2000) An archaeal iron-oxidizing extreme acidophile important in acid mine drainage. *Science* 287: 1796–1799.

Felsenstein J (1985) Confidence limits on phylogenies: an approach using the bootstrap. *Evolution* 39: 783–791.

Gazea B, Adam K & Kontopoulos A (1996) A review of passive systems for the treatment of acid mine drainage. *Miner Eng* 9: 23–42.

Grundl T & Delwiche J (1993) Kinetics of ferric oxyhydroxide precipitation. *J Contam Hydrol* 14: 71–97.

Haig SJ, Collins G, Davies RL, Dorea CC & Quince C (2011) Biological aspects of slow sand filter filtration: past, present and future. *Water Sci Technol* 11: 468–472.

Hallberg KB (2010) New perspectives in acid mine drainage microbiology. *Hydrometallurgy* 104: 448–453.

Harrison G, Curle C & Laishley EJ (1984) Purification and characterization of an inducible dissimilatory type sulfite reductase from *Clostridium pasteurianum*. *Arch Microbiol* 138: 72–78.

Huang Y, Niu B, Gao Y, Fu L & Li W (2010) CD-HIT Suite: a web server for clustering and comparing biological sequences. *Bioinformatics* 26: 680.

Huber T, Faulkner G & Hugenholtz P (2004) Bellerophon; a program to detect chimeric sequences in multiple sequence alignments. *Bioinformatics* 20: 2317–2319.

Hugenholtz P, Pitulle C, Hershberger KL & Pace NR (1998) Novel division level bacterial diversity in a Yellowstone hot spring. *J Bacteriol* 180: 366–376.

Johnson DB & Hallberg KB (2002) Pitfalls of passive mine water treatment. *Rev Environ Sci Biotechnol* 1: 335–343.

Johnson DB & Hallberg KB (2005a) Acid mine drainage remediation options: a review. *Sci Total Environ* 338: 3–14.

Johnson DB & Hallberg KB (2005b) Biogeochemistry of the compost bioreactor components of a composite acid mine drainage passive remediation system. *Sci Total Environ* 338: 81–93.

Kalin M, Fyson A & Wheeler WN (2006) The chemistry of conventional and alternative treatment systems for the neutralization of acid mine drainage. *Sci Total Environ* 366: 395–408.

Kargu F & Uygur A (2003) Effect of carbon source on biological nutrient removal in a sequencing batch reactor. *Bioresour Technol* 89: 89–93.

Kim SD, Kilbane JJ & Cha DK (1999) Prevention of acid mine drainage by sulfate reducing bacteria: organic substrate addition to mine waste piles. *Environ Eng Sci* 16: 139 .

Kimura M (1980) A simple method for estimating evolutionary rates of base substitutions through comparative studies of nucleotide sequences. *J Mol Evol* 16: 111–120.

Macías F, Carabello MA, Nieto JM, Rötting TS & Ayora C (2012) Natural pretreatment and passive remediation of highly polluted acid mine drainage. *J Environ Manage* 104: 93–100.

Marchesi JR, Sato T, Weightman AJ, Martin TA, Fry JC, Hiom SJ & Wade WG (1998) Design and evaluation of useful bacterial primers that amplify genes coding for bacterial 16S rRNA. *Appl Environ Microbiol* 64: 795–799.

McCauley CA, O'Sullivan AD, Mike MW, Weber PA & Trumm DA (2009) Sulfate and metal removal in bioreactors treating acid mine drainage dominated with iron and aluminium. *Water Res* 43: 961–970.

Mulopo J, Greben H, Sigama J, Radebe V, Mashego M & Burke L (2011) The relationships between sulphate reduction and COD/VFA utilisation using grass cellulose as carbon and energy sources. *Appl Biochem Biotechnol* 163: 393–403.

Nocker A, Burr M & Camper AK (2007) Genotypic microbial community profiling: a critical technical review. *Microb Ecol* 54: 276–289.

Obaja D, Macé S & Mata-Alvarez J (2005) Biological nutrient removal by a sequencing batch reactor (SBR) using an internal organic carbon source in digested piggery wastewater. *Bioresour Technol* 96: 7–14.

Osborn AM, Moore ER & Timmis KN (2000) An evaluation of terminal-restriction fragment length polymorphism (T-RFLP) analysis for the study of microbial community structure and dynamics. *Environ Microbiol* 2: 39–50.

Potgieter-Vermaak S, Potgieter JH, Monama P & Van Grieken R (2006) Comparison of limestone, dolomite and fly ash as pre-treatment agents for acid mine drainage. *Miner Eng* 19: 454–462.

Pruesse E, Peplies J & Glöckner FO (2012) SINA: accurate high-throughput multiple sequence alignment of ribosomal RNA genes. *Bioinformatics* 28: 1823–1829.

Ramond J-B, Berthe T, Duran R & Petit F (2009) Comparative effects of mercury contamination and wastewater effluent input on Gram-negative *merA* gene abundance in mudflats of an anthropized estuary (Seine, France): a microcosm approach. *Res Microbiol* 160: 10–18.

Ramond J-B, Welz PJ, Cowan DA & Burton SG (2012) Microbial community structure stability, a key parameter in monitoring the development of constructed wetland mesocosms during start-up. *Res Microbiol* 163: 28–35.

Ramond J-B, Welz PJ, Tuffin MI, Burton SG & Cowan DA (2013) Assessment of temporal and spatial evolution of bacterial communities in a biological sand filter mesocosm treating winery wastewater. *J Appl Microbiol* 115: 91–101.

Reifler RG, Krohn J, Stuart B & Socotch C (2008) Role of sulphur-reducing bacteria in a wetland system treating acid mine drainage. *Sci Total Environ* 394: 222–229.

Reysenbach A-L & Pace NR (1995) Reliable amplification of hyperthermophilic archaeal 16S rRNA genes by PCR. *Archaea: A Laboratory Manual – Thermophiles* (Robb FT & Place AR, eds), pp. 101–107. Cold Spring Harbour Laboratory Press, New York, NY.

Saitou N & Nei M (1987) The neighbor-joining method: a new method for reconstructing phylogenetic trees. *Mol Biol Evol* 4: 406–425.

Schröder I, Johnson E & de Vries S (2003) Microbial ferric iron reductases. *FEMS Microbiol Rev* 27: 427–447.

Sercu B, van de Werfhorst LC, Murray JLS & Holden PA (2011) Cultivation-independent analysis of bacteria in IDEXX quanti-tray/2000 fecal indicator assays. *Appl Environ Microbiol* 77: 627–633.

Sheoran AS, Sheoran V & Choudhary RP (2010) Bioremediation of acid-rock drainage by sulphate-reducing prokaryotes: a review. *Miner Eng* 23: 1073–1100.

Tamura K, Peterson D, Peterson N, Stecher G, Nei M & Kumar S (2011) MEGA5: molecular evolutionary genetics analysis using maximum likelihood, evolutionary distance,and maximum parsimony methods. *Mol Biol Evol* 28: 2731–2739.

Tyson GX, Lo I, Baker BJ, Allen EE, Hugenholtz P & Banfield JF (2005) Genome-directed isolation of the key nitrogen fixer *Leptospirulum ferrodiazotrophum* sp. nov. from an acidophilic microbial community. *Appl Environ Microbiol* 71: 6319–6324.

Welz PJ, Ramond J-B, Cowan DA & Burton SG (2012) Phenolic removal processes in biological sand filters, sand columns and microcosms. *Bioresour Technol* 119: 262–269.

Wilkin RT (2008) Contaminant attenuation processes at mine sites. *Mine Water Environ* 27: 251–258.

Supporting Information

Additional Supporting Information may be found in the online version of this article: Fig. S1. X-ray diffraction (XRD) spectra of the BSF sediments (dark blue) compared with the spectra of quartz (a), quartz/carbonates (b) and quartz/aluminosilicates (c). Fig. S2. Venn diagrams showing the distribution of T-RFs present in the BSF surface sediments at the inlet (a) and outlet (b). Fig. S3. Venn diagrams showing the distribution of T-RFs present in the BSF deep sediments at the inlet (a) and the outlet (b). Table S1. Taxonomic classification of the clones from AMD-impacted surface BSF sediments using the online SINA aligner with the default parameters (http://www. arb-silva.de/aligner; Pruesse *et al.*, 2012). Table S2. Taxonomic classification of the clones from AMD-impacted BSF deep sediments using the online SINA aligner with the default parameters (http://www.arb-silva.de/aligner; Pruesse *et al.*, 2012).